

62511585
11034

Y3, N21/516/2054

NACA TN 2054

NATIONAL ADVISORY COMMITTEE FOR AERONAUTICS

TECHNICAL NOTE 2054

STRESS AND DISTORTION MEASUREMENTS IN A 45° SWEEP
BOX BEAM SUBJECTED TO ANTISYMMETRICAL
BENDING AND TORSION

By George W. Zender and Richard R. Heldenfels

Langley Aeronautical Laboratory
Langley Air Force Base, Va.



Washington

April 1950

CONN. STATE LIBRARY

APR 10 1950

BUSINESS, SCIENCE
& TECHNOLOGY DEPT.

NATIONAL ADVISORY COMMITTEE FOR AERONAUTICS

TECHNICAL NOTE 2054

STRESS AND DISTORTION MEASUREMENTS IN A 45° SWEEP
BOX BEAM SUBJECTED TO ANTISYMMETRICAL
BENDING AND TORSION

By George W. Zender and Richard R. Heldenfels

SUMMARY

An untapered aluminum-alloy box beam, representing the main structural component of a full-span, two-spar, 45° swept wing with a carry-through section, was subjected to antisymmetrical tip bending and twisting loads such that the stresses were kept below the proportional limit.

The investigation revealed that the antisymmetrical loading magnified the effects of sweep which were previously observed for symmetrical loads on the same box beam. The effects are a build-up of normal stress and vertical shear stress in the rear spar near the fuselage when the box beam is considered sweptback. An additional result of antisymmetrical loading was the appearance of large shear-lag stresses in the carry-through section, particularly in the bending case.

The investigation further revealed that the spar deflections of the swept box beam could be estimated by an approximate method of analysis; however, this method is less accurate for antisymmetrical than for symmetrical bending loads because of the shear-lag effects in the carry-through section.

INTRODUCTION

The stresses and distortions of a 45° swept box beam loaded by symmetrical tip bending and tip twisting loads are presented in reference 1 and an approximate method of evaluating the deflections is given. The test specimen used to obtain the data of reference 1 (see fig. 1) was again tested with antisymmetrical tip bending and tip twisting loads applied and the results are presented in this paper. The stresses for the antisymmetrical loadings are compared with standard beam formulas and the distortions with those obtained from the approximate method of reference 1.

SYMBOLS

A	area enclosed by cross section, square inches
E	Young's modulus of elasticity (10,500 ksi)
G	shear modulus of elasticity (4000 ksi)
I	geometric moment of inertia, inches ⁴
I _o	geometric moment of inertia of outer bays of carry-through section, inches ⁴
J	torsional stiffness constant, inches ⁴
R	reaction of conjugate beam, kips
L	length, inches
M	bending moment, kip-inches
P	load, kips
Q	area moment, inches ³
T	torque, kip-inches
V	shear force, kips
b	width of box beam, inches
c	distance from neutral axis to any fiber, inches
h	depth of spar web, inches
l	length of carry-through section, inches
t	thickness, inches
t _a	thickness of spar web, inches
x	distance from origin for antisymmetrical tip bending loads, inches
x'	distance from origin for antisymmetrical tip torques, inches
y _F	deflection of front spar, inches

y_R	deflection of rear spar, inches
α	total rotation at ends of carry-through section, radians
α_1	rotation at end of carry-through section due to shear distortion, radians
α_2	rotation at end of carry-through section due to bending distortion, radians
γ_a	shear strain of spar web
θ	rotation of cantilever portion due to flexibility of triangular bay, radians
σ	longitudinal stress, ksi
τ	shear stress, ksi
ϕ	rotation of cross section due to torque, radians
Λ	angle of sweep, degrees

TEST SPECIMEN

The pertinent details of the swept box beam are shown in figure 2. (Hereinafter the box beam is referred to as sweptback rather than swept; thus the spars (or sidewalls) may be conveniently referred to as "front" and "rear" without ambiguity.) The sweptback parts consisted of two boxes with their longitudinal axes at right angles, joined by and continuous with a short rectangular carry-through section representing that part of a wing to be found inside an airplane fuselage. The material of the specimen was 24S-T3 aluminum alloy except for the bulkheads. The bulkheads consisted of rectangular steel sheets with a 90° bend at each edge, forming flanges for attachment to the spars and covers. Bulkheads 2, 3, 4, and 5 were $\frac{3}{32}$ -inch thick, whereas all other bulkheads were $\frac{1}{8}$ -inch thick.

The cover sheet and front spar web, but not the rear spar web, were spliced at the center line of the carry-through section, and the stringers and spar flanges were spliced at the ends of the carry-through section, as shown in figure 2. The front and rear spars were also reinforced at the ends of the carry-through section where the box beam was supported.

METHOD OF TESTING

The setup for the antisymmetrical tip-bending test is shown in figure 1. For the antisymmetrical tip-twisting test the setup was the same as shown in figure 2 of reference 1 except that the torque at the left side of the wing was applied in the opposite direction. The box was supported by steel rollers, with axes parallel to the direction of flight, at the four corners of the carry-through section, and loads were applied at the tips of the box. (The bulkheads at the ends of the carry-through section and the vertical reactions provided by the rollers taken together were assumed to represent the restraint that might be provided by a fuselage to the wing.) All loads were applied at the tips by means of hydraulic jacks. At each tip the load was transferred from the jack to the tip bulkhead in such a manner that the resultant load applied to the box was a vertical force acting through the center of the tip cross section for bending or a pure torque acting in the plane of the tip cross section for torsion.

Forces exerted by the hydraulic jacks were measured by means of dynamometers. Strains were measured on the top cover and the side walls in the carry-through section and on the right side of the box beam by means of Tuckerman optical strain gages. Stringer and flange strains were converted to stresses by use of a value of $E = 10,500$ ksi; shear stresses were obtained from shear strains by use of a value of $G = 4,000$ ksi. Spar deflections were measured by means of dial gages along the top flanges of the spars and, at the support stations, the deflections of the center lines of the spar webs were measured with optical micrometers.

RESULTS

Stresses due to antisymmetrical bending.- The normal stresses in the stringers and flanges due to tip bending loads of 2.5 kips are shown in figure 3 and are compared with the stresses given by the formula $\frac{Mc}{I}$ of elementary beam theory, shown by means of dashed lines. The top cover and spar shear stresses due to the same bending loads are shown in figure 4 and are compared with the stresses $\frac{VQ}{It}$ of elementary beam theory.

Stresses due to antisymmetrical torsion.- The stringer and flange stresses due to antisymmetrical tip torques of 43.42 kip-inches are plotted in figure 5. The stringer and flange stresses in the carry-through section of the box beam in figure 5 are compared with

the $\frac{Mc}{I}$ stress due to the component of the tip torque which produces bending of the carry-through section. The shear stresses in the top cover and spar webs due to the same antisymmetrical tip torques are given in figure 6 and are compared with the stresses $\frac{T}{2At}$ and $\frac{VQ}{It}$ of ordinary shell theory.

Distortions due to antisymmetrical bending.- The experimental spar deflections (adjusted for support deflections as explained in the section entitled "Effects of Support Deflections") due to antisymmetrical tip bending loads of 2.5 kips are given in figure 7(a) and are compared with theoretical spar deflections shown by means of dashed curves. The theoretical deflection curves were obtained by assuming the outer section to be clamped as a cantilever at bulkhead 6 and superimposing on the cantilever deflections the estimated deflections of the outer section due to the flexibility of the triangular and the carry-through sections. A detailed description of these computations is contained in appendix A.

The experimental and theoretical spar deflections shown in figure 7(a) were used to calculate the rotations (in their own planes) of cross sections perpendicular to the spars and cross sections parallel to the direction of flight. These cross-sectional rotations are shown in figure 7(b).

Distortions due to antisymmetrical torsion.- The experimental spar deflections (adjusted for support deflections as explained in the section entitled "Effects of Support Deflections") due to antisymmetrical twisting moments of 43.42 kip-inches are given in figure 8(a) and are compared with theoretical spar deflections, shown by means of dashed curves, obtained by applying ordinary torsion theory $\frac{d\phi}{dx} = \frac{T}{GJ}$ to the outer section of the beam and then superimposing rigid-body translations and rotations due to the flexibility of the triangular and carry-through sections. The details of these computations are in appendix B.

The experimental and theoretical spar deflections shown in figure 8(a) were used to calculate the cross-sectional rotations shown in figure 8(b).

Effect of support deflections.- Since the supporting jig was not rigid, the reaction points deflected for both the antisymmetrical tip bending and torque loads. The effect of these deflections was partially removed from the test data by means of rigid-body displacements and rotations which adjusted the measured deflections to the values presented in figures 7 and 8 without affecting the stresses. Removal of all the support deflections by rigid-body movements was not possible because the carry-through section twisted. The amount of twist remaining after the rigid-body movements is shown in figure 9. This

twist results in stresses and distortions which are slightly different from those which would have been obtained with rigid supports. An analytical correction would require a complete stress and distortion analysis of the box beam which is beyond the scope of this paper.

If the warping resistance of the outboard portion of the box beam is known, however, an approximate correction to the stresses in the carry-through section, where the principal changes would be expected, can be obtained by applying the method of reference 2 to an idealized representation of the carry-through section, which is twisted an amount equal and opposite to that shown in figure 9. Since that warping resistance is unknown, the true solution can be bracketed by two other solutions: The first assumes that the outer part offers no resistance to warping and thus the end of the carry-through sections are free to warp; whereas, the second assumes an infinite warping resistance and thus the ends of the carry-through section do not warp. The values obtained from each of these analyses are listed in the following table as stress corrections which, when applied to the test data, will approximate the values for rigid supports:

Stress correction, ksi				
Type of stress	Antisymmetrical bending		Antisymmetrical torsion	
	Ends free to warp	Ends do not warp	Ends free to warp	Ends do not warp
Cover shear	0.65	0.38	0.09	0.05
Front-spar shear	.42	1.41	.06	.19
Rear-spar shear	-.42	-1.41	-.06	-.19
Front flange	0	-.70	0	-.10
Rear flange	0	.70	0	.10

These corrections apply to the stress at the cross section 10 inches to the right of the center line of the carry-through section in figures 3 to 6. Since the true correction lies somewhere between the two values listed for each loading, the corrections are seen to be so small that adjustment of the experimental stresses of figures 3 to 6 is unnecessary.

DISCUSSION

Stresses due to antisymmetrical bending.- The bending stresses (fig. 4) in the triangular section and outer section of the box for

antisymmetrical tip bending loads are substantially the same as the stresses given in reference 1 for symmetrical tip bending loads. Since the shear lag is more severe in the antisymmetrical tip bending load case, however, near bulkhead 6 and inboard to the carry-through section, the bending stresses are slightly different from those of reference 1 and the shear stresses (fig. 4) are considerably different from those shown in reference 1. The normal stress in the rear spar immediately outboard of bulkhead 6 was 1.6 times the $\frac{Mc}{I}$ stress for the antisymmetrical bending loads as compared to 1.4 for the symmetrical bending loads, whereas the vertical shear stress in the rear spar immediately outboard of bulkhead 6 was 1.64 times the vertical shear stress at the tip for antisymmetrical loads as compared to 1.33 for the symmetrical bending loads.

The principal difference between the stresses for the antisymmetrical and symmetrical tip bending load cases occurred in the carry-through section, as might be expected from the fact that the carry-through section is subjected to both vertical shear and torque in the antisymmetrical case but to neither in the symmetrical case. As shown in figures 3 and 4, the normal and shear stresses in the carry-through sections are considerably different from the stresses obtained from the elementary formulas $\frac{Mc}{I}$ and $\frac{VQ}{It}$. The deviations are due to the torque in the carry-through section and to shear lag. Much better agreement of the test results with $\frac{Mc}{I}$ and $\frac{VQ}{It}$ were obtained in reference 1 because the shear-lag effects in the carry-through section for symmetrical tip bending loads were negligible and no torque was present.

Stresses due to antisymmetrical torsion.- Except for the carry-through section, the stresses due to antisymmetrical tip torques (figs. 5 and 6) are essentially the same as the stresses for symmetrical tip torques presented in reference 1. An appreciable decrease occurs in the shear stresses in the covers and front spar web in the portion of the triangular section nearest the carry-through section. A comparison of figures 3 and 5 and figures 4 and 6 shows that the stresses in the carry-through section are in better agreement with the elementary stresses $\frac{Mc}{I}$ and $\frac{VQ}{It}$ for the tip torsion loads than for the tip bending loads. The better agreement is a result of the different end restraint provided the carry-through section by the triangular section under torsion loads so that the secondary stresses, due to vertical shear and torque (which are not present for symmetrical torsion loads), are a smaller percentage of the elementary stress for the antisymmetrical torsion load than for the antisymmetrical bending load.

Distortions due to antisymmetrical bending.- The distortions due to antisymmetrical tip bending loads (fig. 7) are of greater magnitude than

the distortions given in reference 1 for symmetrical tip bending loads. This is due to the larger end rotation of the carry-through section which results in larger deflections of the outer section of the box beam for antisymmetrical than for symmetrical tip bending loads. The bending moment applied to the carry-through section caused it to deflect into one half-wave for the symmetrical bending load, although two half-waves were formed for the antisymmetrical bending load. This action alone would result in a lesser rotation; however, the large vertical shear present in the latter case caused sufficient shear deformation of the spar webs to result in a larger total end rotation of the carry-through section for antisymmetrical than for the symmetrical tip bending loads.

The distortions are computed in the same manner as in reference 1 except that in this paper the carry-through section is analyzed for antisymmetrical loads in order to include the types of distortion previously described.

The detailed computations of the deflections are given in appendix A and are compared with experimental deflections in figure 7(a). The comparison of the experimental and theoretical deflections indicates that the carry-through section is more flexible for antisymmetrical bending loads than is indicated by the approximate method of evaluating the deflections. This result is primarily due to the large shear lag present in the carry-through section which permits a larger rotation at the ends of the carry-through section due to bending than is given by the elementary beam theory used in appendix A. Also, the difference of the deflections of the front spar and rear spar at any station x of figure 7(a) is larger experimentally than theoretically. This effect is reflected in figure 7(b) where the rotations perpendicular to the spars are larger experimentally than theoretically. The disagreement between theory and experiment here, in addition to the influence of shear lag of the carry-through section, is the result of an indeterminate amount of bending of bulkhead 6 in its own plane as well as the rate of twist caused by the warping of the cross section at bulkhead 6 and the twist of the carry-through section.

Distortions due to antisymmetrical torsion.- Figure 8 shows good agreement of the experimental distortions and those calculated in appendix B. Better agreement between experiment and the approximate method is obtained here than in the antisymmetrical bending case because the shear-lag effects were smaller in the carry-through section.

CONCLUSIONS

The following conclusions apply to an untapered, aluminum-alloy, 45° sweptback box beam of the type for which test results are reported in this paper. The box beam was constructed to represent the main structural component of a full-span, two-spar, 45° swept wing with a rectangular carry-through section and with bulkheads placed perpendicular to the spars. The conclusions are based on tests in which the loading was applied antisymmetrically with respect to the carry-through section and consisted of vertical forces (bending loads) and torques (twisting loads) applied in the planes of the two tip cross sections. A cross section should be understood to mean a section cut by a plane perpendicular to the spars or side walls. Comparisons of antisymmetrical with symmetrical load results are based upon symmetrical load data obtained from the same sweptback box beam but presented in a previous paper.

1. The main effect of antisymmetrical tip bending loads on the stresses is to produce a greater concentration of normal stress and vertical shear in the rear spar at the cross section immediately outboard of the carry-through section than for symmetrical tip bending loads and to introduce large shear lag effects in the carry-through section. For antisymmetrical bending loads the carry-through section is subject to vertical shear and torque which are not present for symmetrical bending loads.

2. The most marked feature of the stresses due to antisymmetrical torque loads, as in the case of symmetrical torque loads, is an appreciable decrease in the shear stresses in the covers and front spar in that portion of the triangular section nearest the carry-through section. For antisymmetrical torsion loads the carry-through section is subject to vertical shear and torque which are not present for symmetrical torsion loads.

3. The spar deflections of the sweptback box beam can be estimated approximately by considering the outboard portions to be cantilevers and superimposing on the cantilever deflections rigid-body movements due to the flexibility of the inboard region to which the cantilevers are attached. The deflections obtained by this method are less accurate

for antisymmetrical than for symmetrical bending loads because of the shear-lag effects in the carry-through section.

Langley Aeronautical Laboratory
National Advisory Committee for Aeronautics
Langley Air Force Base, Va., January 9, 1950

APPENDIX A

CALCULATIONS FOR DISTORTIONS DUE TO ANTISYMMETRICAL
TIP BENDING LOADS

The theoretical spar deflections plotted in figure 7(a) are the sum of four separately calculated component deflections. The first three component deflections are identical to those given in appendix A of reference 1, but the fourth component deflection, which is that due to the flexibility of the carry-through section, differs from that of reference 1 in that the carry-through section is loaded differently.

The first three components of the total spar deflections are explained in detail in appendix A of reference 1. These components and the resulting equations for the deflections of the outer section are:

The cantilever deflection of the outer section

$$y_F = y_R = \frac{PL^3}{EI} \left[\frac{1}{2} \left(\frac{x}{L} \right)^2 - \frac{1}{6} \left(\frac{x}{L} \right)^3 \right]$$

$$= 0.440x^2(267 - x)10^{-6} \text{ inches} \quad (A1)$$

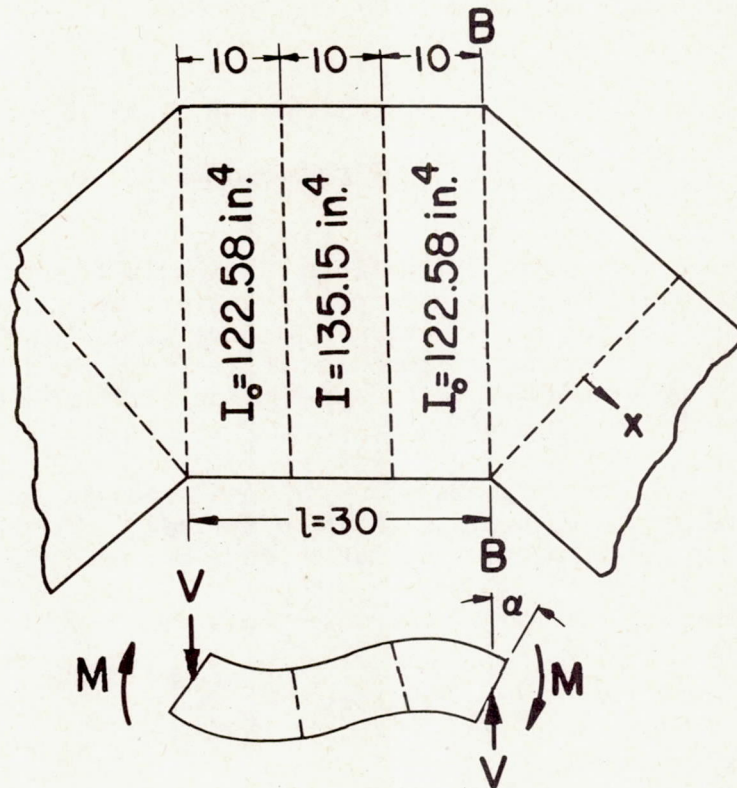
the spar shear deflection of the outer section

$$y_F = y_R = \gamma_a x = \frac{P}{2ht_a G} x = 0.000572x \text{ inches} \quad (A2)$$

and the deflection of the outer section due to flexibility of the triangular section

$$y_F = y_R = \theta x = 0.00353x \text{ inches} \quad (A3)$$

The fourth component of the total spar deflections is that due to the flexibility of the carry-through section, which is assumed to contribute to the cantilever a rotation α about the axis B-B. (See the following sketch.)

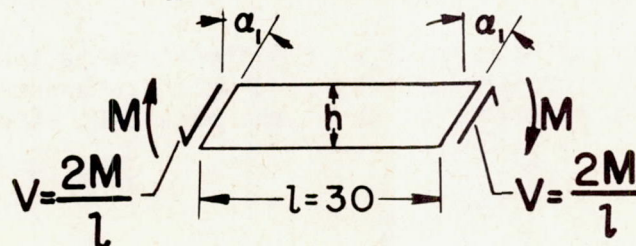


This rotation is assumed to consist of two parts which are evaluated in this appendix. The first part is the rotation due to the shear distortion of the spar webs and the second part is the rotation due to the bending distortion. The rotation of the carry-through section is then obtained by superposition of the two parts.

Rotation due to shear distortion of spar webs. Equilibrium requires that the shear V in the carry-through section be

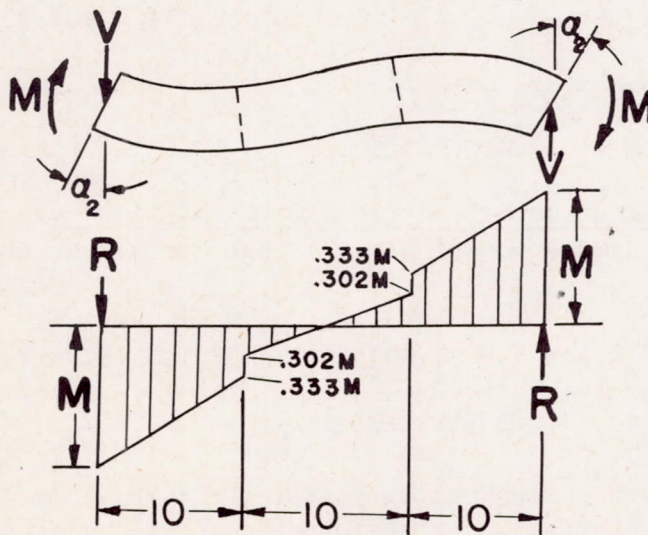
$$V = \frac{2M}{l}$$

and that the rotation α_1 due to the shear distortion (see sketch) be



$$\begin{aligned} \alpha_1 &= \frac{V}{2ht_aG} = \frac{M}{ht_aG\ell} \\ &= \frac{M}{(7)(0.078)(4 \times 10^3)(30)} \\ &= 0.01526 \times 10^{-3}M \end{aligned}$$

Rotation due to bending distortion.- Since the carry-through section is composed of bays of different stiffnesses, the conjugate beam method is a convenient way of evaluating the rotation α_2 due to the bending distortion. The loading of the conjugate beam is the moment of the actual structure with the moment in the center bay reduced by the ratio $\frac{I_0}{I} = \frac{122.58}{135.15}$ in order to account for the increased moment of inertia of the center bay (See reference 3.) The resulting loading is shown in the following sketch:



The rotation of the actual beam at any cross section is equal to the shear of the conjugate beam at that cross section divided by EI_0 . The

rotation α_2 at the end of the carry-through section due to the bending distortion of the carry-through section is therefore

$$\begin{aligned}\alpha_2 &= \frac{R}{EI_0} \\ &= \frac{1}{(10,500)(122.58)} \frac{2}{30} \left[\frac{5}{2}(0.302M)\frac{10}{3} + 10(0.333M)10 + \frac{0.667M(10)\frac{35}{3}}{2} \right] \\ &= 0.00387 \times 10^{-3}M\end{aligned}$$

Superposition of rotation due to shear distortion and rotation due to bending distortion.- Adding the rotations due to shear and bending distortion to obtain the total rotation of the carry-through section due to end moment M gives

$$\alpha = \alpha_1 + \alpha_2 = 0.01913M \times 10^{-3}$$

For the experimental swept box beam, the moment on the carry-through section is

$$M = P(L + 15)\cos \Lambda = 2.5(89 + 15)(0.707) = 183.82 \text{ inch-kips}$$

and the rotation α is therefore

$$\alpha = 0.01913(183.82)10^{-3} = 0.003518 \text{ radian}$$

Deflections of outer section due to rotation α .- The spar deflections produced by the rotation α of the cantilever about axis B-B are then

$$\left. \begin{aligned}y_F &= \alpha(x + 30)\cos \Lambda = (0.00352)(x + 30)(0.707) = 0.00249(x + 30) \\ y_R &= \alpha x \cos \Lambda = (0.00352)(x)(0.707) = 0.00249x\end{aligned} \right\} (A4)$$

For antisymmetrical tip bending loads, the total spar deflections are obtained by adding the individual spar deflections as calculated by equations (A1), (A2), and (A3) and equation (A4). The calculated individual deflections and the total deflections for several stations along the spars are listed in the following table:

Type of deflection (deflection measured in in.) (a)	Spar	x (in.)				
		0	20	40	60	80
Cantilever deflection (equation (A1))	Front	0	0.0435	0.1598	0.3278	0.5265
	Rear	0	.0435	.1598	.3278	.5265
Deflection due to spar shear (equation (A2))	Front	0	.0114	.0229	.0343	.0458
	Rear	0	.0114	.0229	.0343	.0458
Deflection due to flexibility of triangular section (equation (A3))	Front	0	.0706	.1412	.2118	.2824
	Rear	0	.0706	.1412	.2118	.2824
Deflection due to flexibility of carry-through section (equation (A4))	Front	.0747	.1244	.1742	.2240	.2739
	Rear	0	.0498	.0996	.1494	.1992
Total deflection	Front	.0747	.2499	.4981	.7979	1.1286
	Rear	0	.1753	.4235	.7233	1.0539

^aPositive deflection downward.

The total deflections of the front and rear spars given in the last row of the table are plotted in figure 7(a).

According to the assumptions made, rotations (in their own planes) of cross sections perpendicular to the spars result only from the flexibility of the carry-through sections. These rotations are constant along the span and can be calculated by dividing the difference between the rear and front spar deflections at any station by the width of the box; therefore, the rotation is $\frac{-0.0747}{30} = -0.00249$ radian. This value is plotted as the horizontal dashed line in figure 7(b).

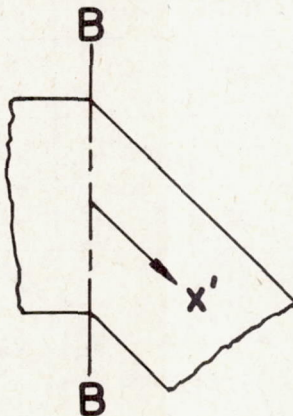
APPENDIX B

CALCULATIONS FOR DISTORTIONS DUE TO

ANTISYMMETRICAL TIP TORQUES

As in the bending case, the theoretical spar deflections plotted in figure 8(a) are the sum of four separately calculated component deflections, the first three of which are identical to the first three component deflections given in appendix B of reference 1. The fourth component deflection, which is that due to the flexibility of the carry-through section, is the same as that of appendix A of this paper except for the magnitude of the applied moments.

The first three component deflections of the spars of the outer section are explained in detail in appendix B of reference 1. Herein x' is measured from the center of cross section B-B as shown in the following sketch:



These three components and the resulting equations for the deflections of the outer section are:

The deflection of the outer section due to elementary twisting

$$-y_F = y_R = \frac{T x'}{GJ} \frac{b}{2} = 0.001278 x' \text{ inches} \quad (B1)$$

the rigid body translation to give zero deflection at supports

$$y_F = y_R = -0.01917 \text{ inch} \quad (B2)$$

and the deflection of the outer section to establish continuity with the triangular section

$$y_F = y_R = -0.00061(x' - 15) \text{ inches}$$

for

$$x' \geq 15 \quad (B3)$$

The fourth component of the total spar deflections is that due to the flexibility of the carry-through section, which is assumed to contribute to the cantilever a rotation α about axis B-B. The equation for the rotation α in appendix A may be used with M replaced by

$$\begin{aligned} -T \sin \Lambda &= -(43.42)(0.707) \\ &= -30.7 \text{ inch-kips} \end{aligned}$$

with the result that

$$\alpha = 0.01913 (-30.7) \times 10^{-3} = -0.0005875 \text{ radian}$$

The corresponding front and rear spar deflections are, respectively,

$$\left. \begin{aligned} y_F &= \alpha(x' + 15) \cos \Lambda = -0.0005875(x' + 15)(0.707) \\ &= -0.0004153(x' + 15) \\ y_R &= \alpha(x' - 15) \cos \Lambda \\ &= -0.0004153(x' - 15) \end{aligned} \right\} (B4)$$

The total spar deflections are obtained by superimposing the component spar deflections given by equations (B1) to (B4). These component deflections and the total deflections are listed in the following table for two stations:

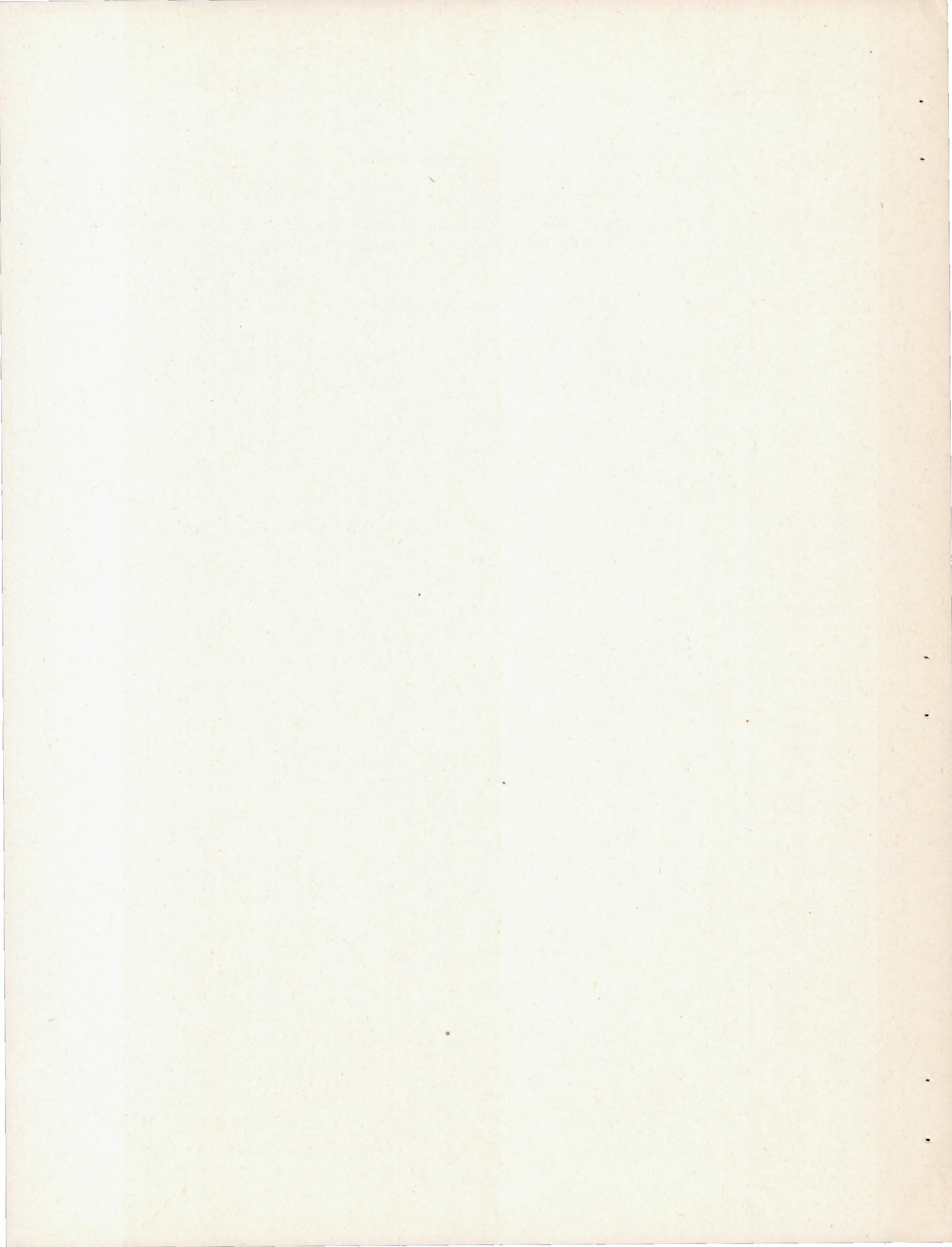
Type of deflection (deflection measured in in.) (a)	Spar	x' (in.)	
		20	100
Deflection due to elementary twisting (equation (B1))	Front	-0.0256	-0.1278
	Rear	.0256	.1278
Rigid-body translation to give zero deflection at supports (equation (B2))	Front	-.0192	-.0192
	Rear	-.0192	-.0192
Deflection to establish continuity with triangular section (equation (B3))	Front	-.0031	-.0519
	Rear	-.0031	-.0519
Deflection due to flexibility of carry-through section (equation (B4))	Front	-.0145	-.0478
	Rear	-.0021	-.0353
Total deflection	Front	-.0624	-.2467
	Rear	.0012	.0214

^aPositive deflection downward.

Since the equations for the spar deflections are linear in x' , the total deflections are given by the straight lines of figure 8(a).

REFERENCES

1. Zender, George, and Libove, Charles: Stress and Distortion Measurements in a 45° Swept Box Beam Subjected to Bending and to Torsion. NACA TN 1525, 1948.
2. Kuhn, Paul: A Method of Calculating Bending Stresses Due to Torsion. NACA ARR, Dec. 1942.
3. Timoshenko, S.: Strength of Materials. Part I - Elementary Theory and Problems. D. Van Nostrand Co., Inc., 1930.



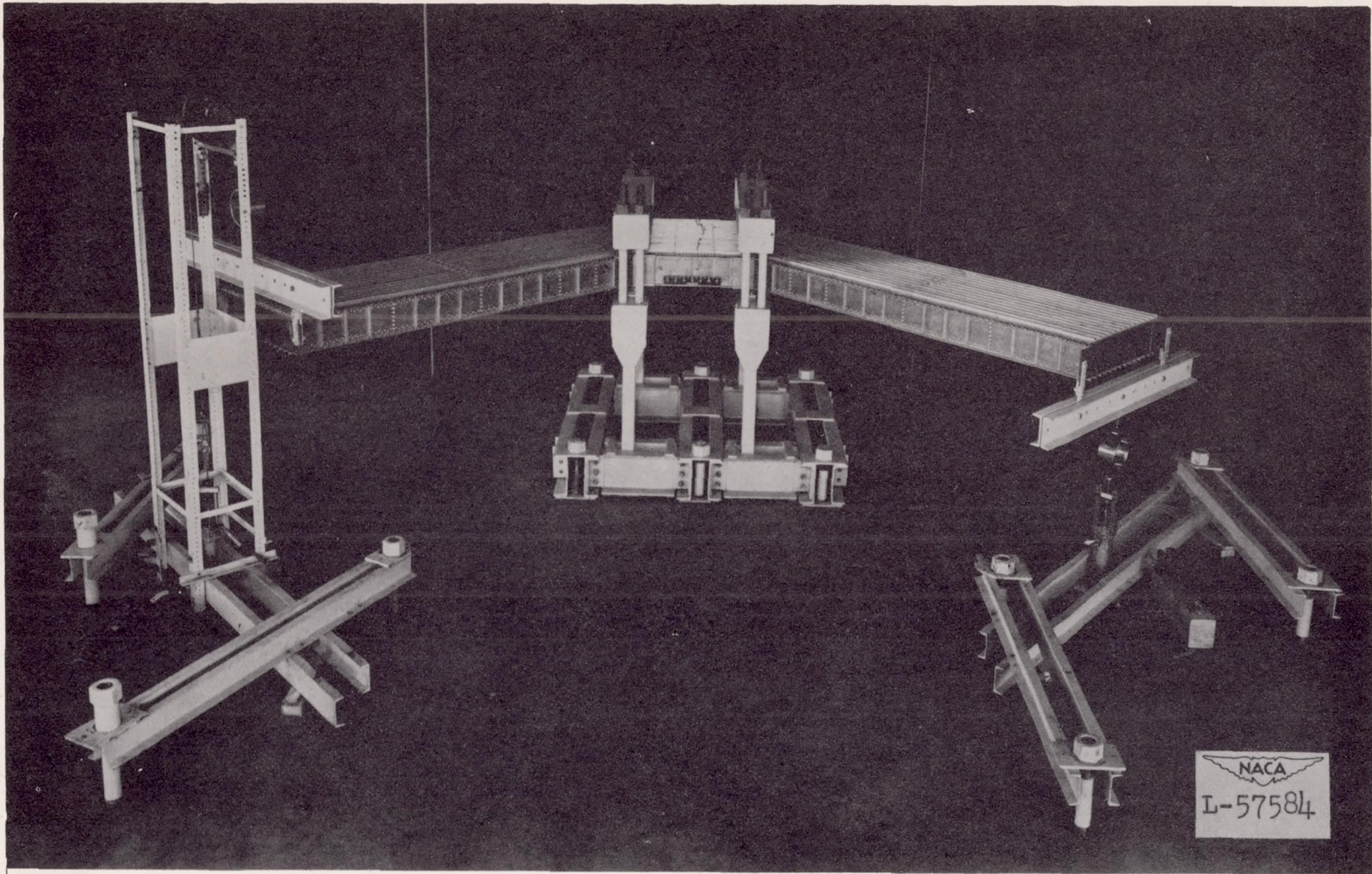
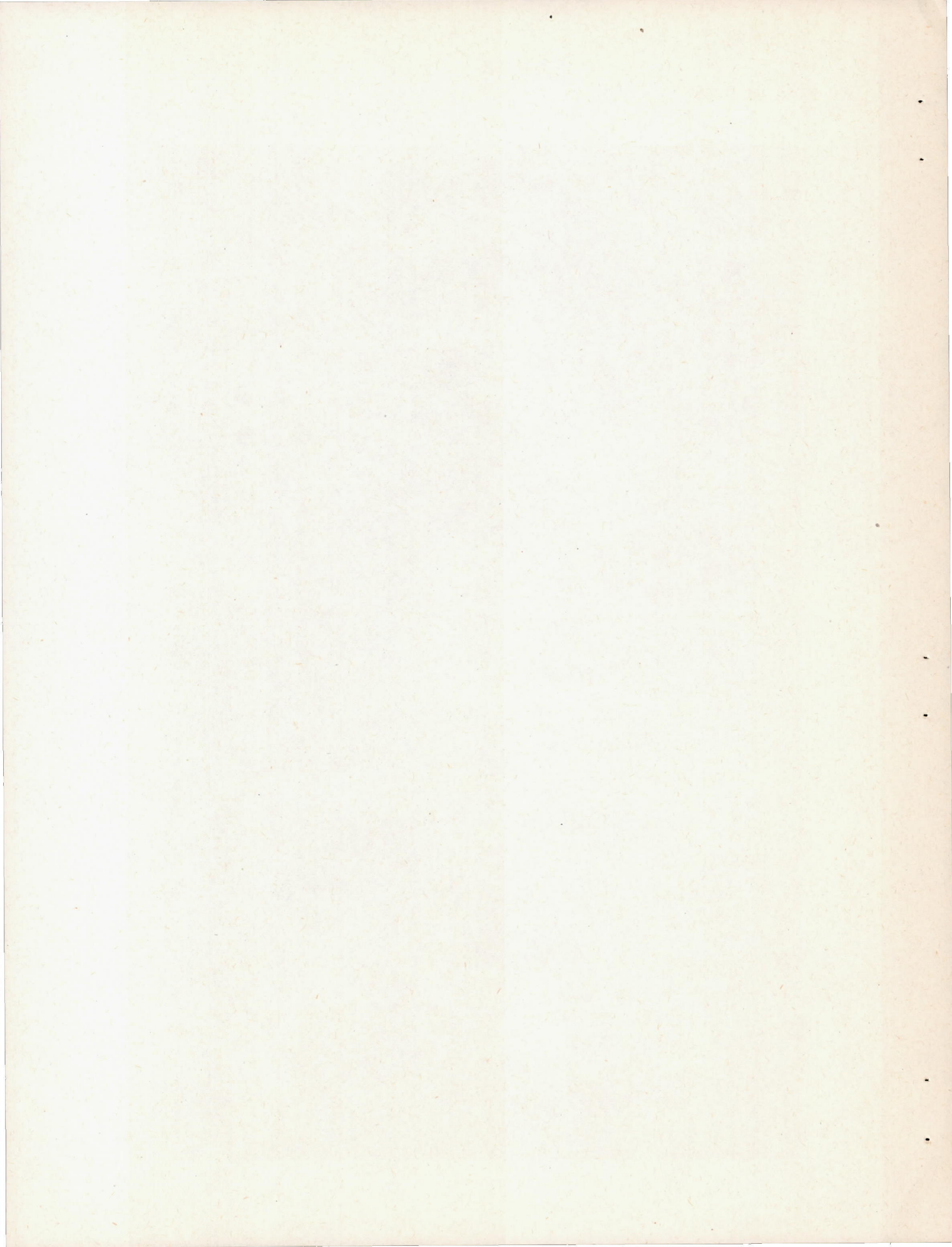


Figure 1.- Antisymmetrical bending test setup of sweptback box beam.



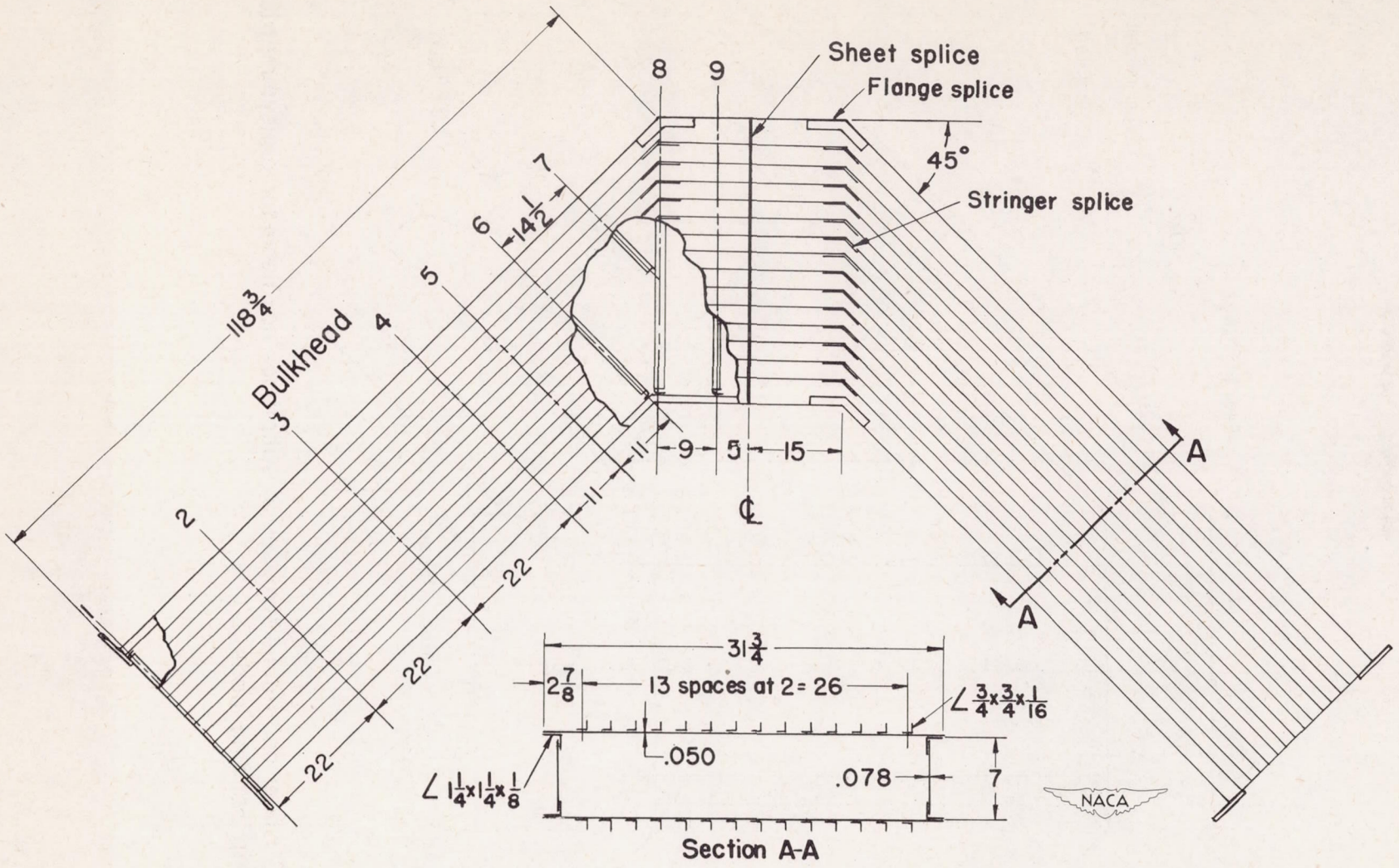


Figure 2.- Details of sweptback box beam.

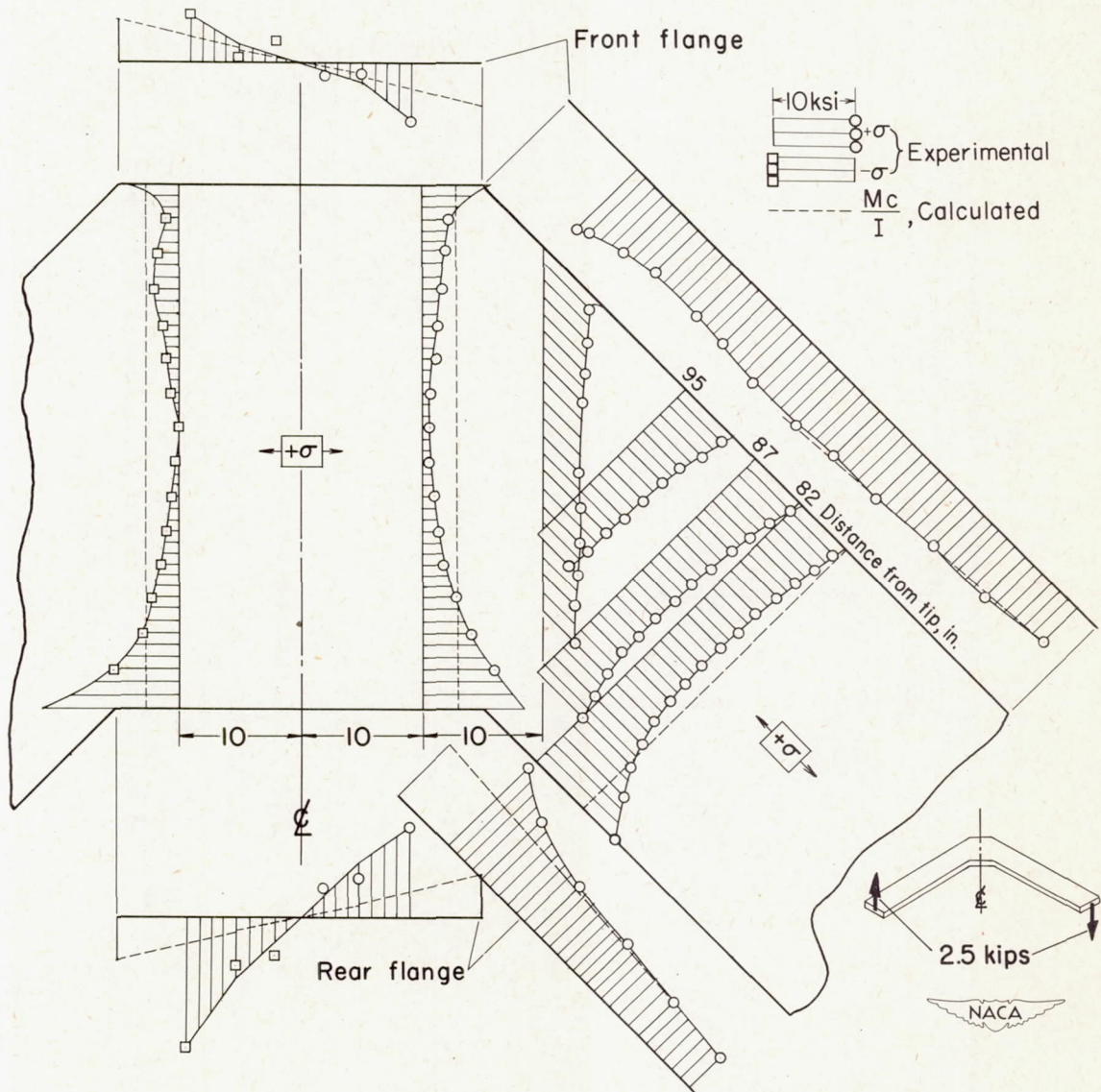


Figure 3-Stringer and flange stresses of sweptback box beam for antisymmetrical tip bending loads.

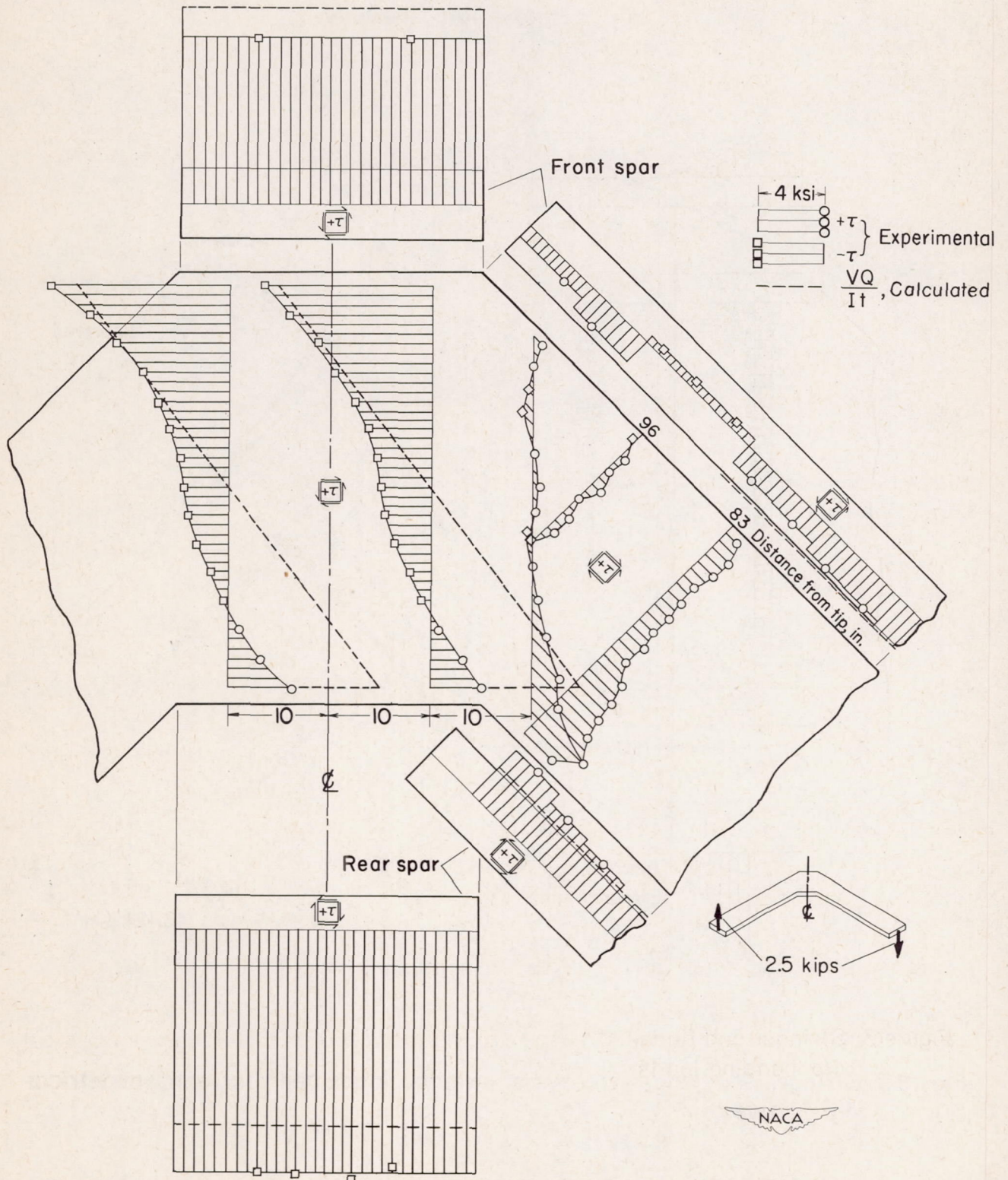


Figure 4. Shear stresses in top cover and spar webs of sweptback box beam for antisymmetrical tip bending loads.

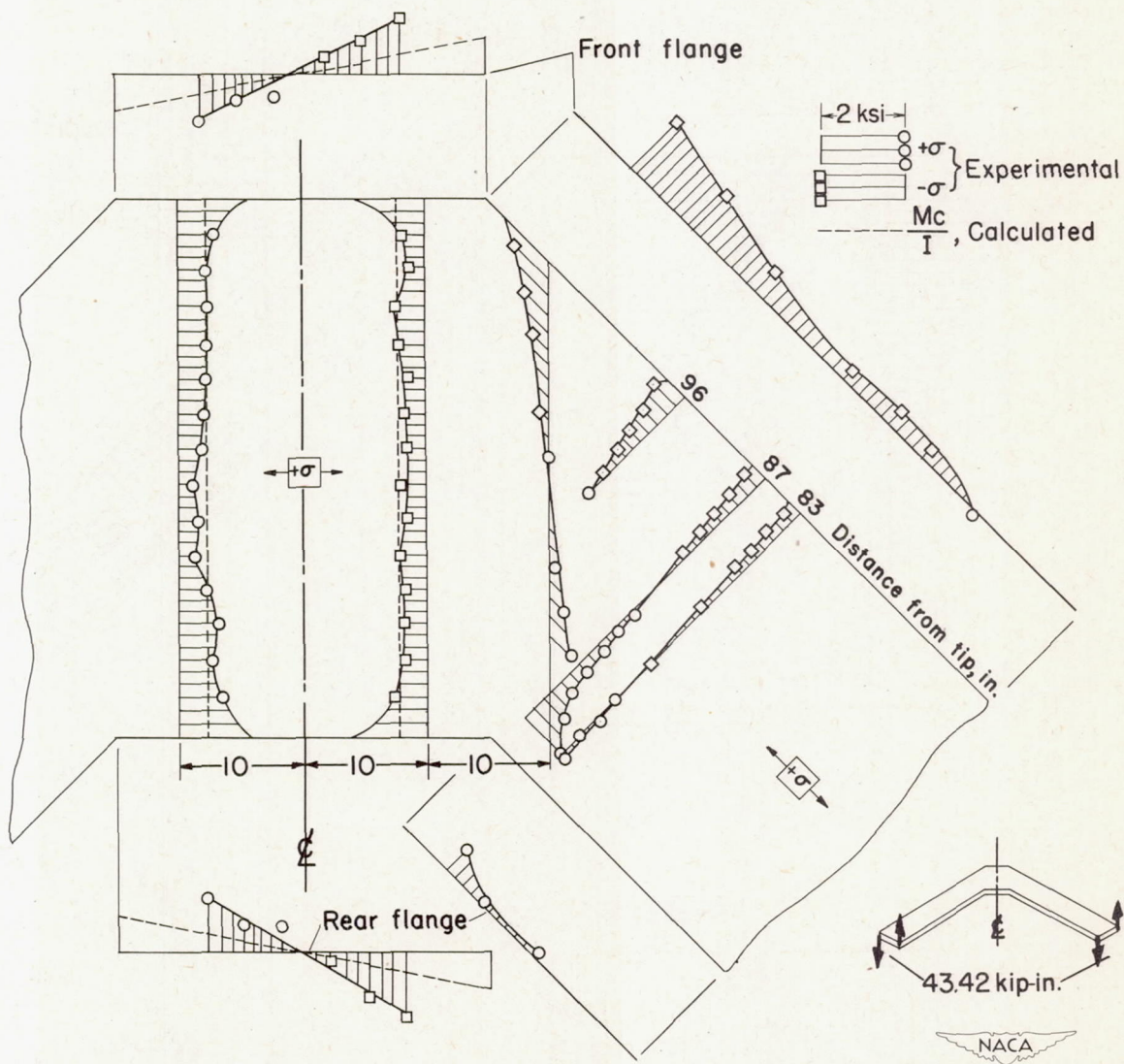


Figure 5.-Stringer and flange stresses of sweptback box beam for antisymmetrical tip torques.

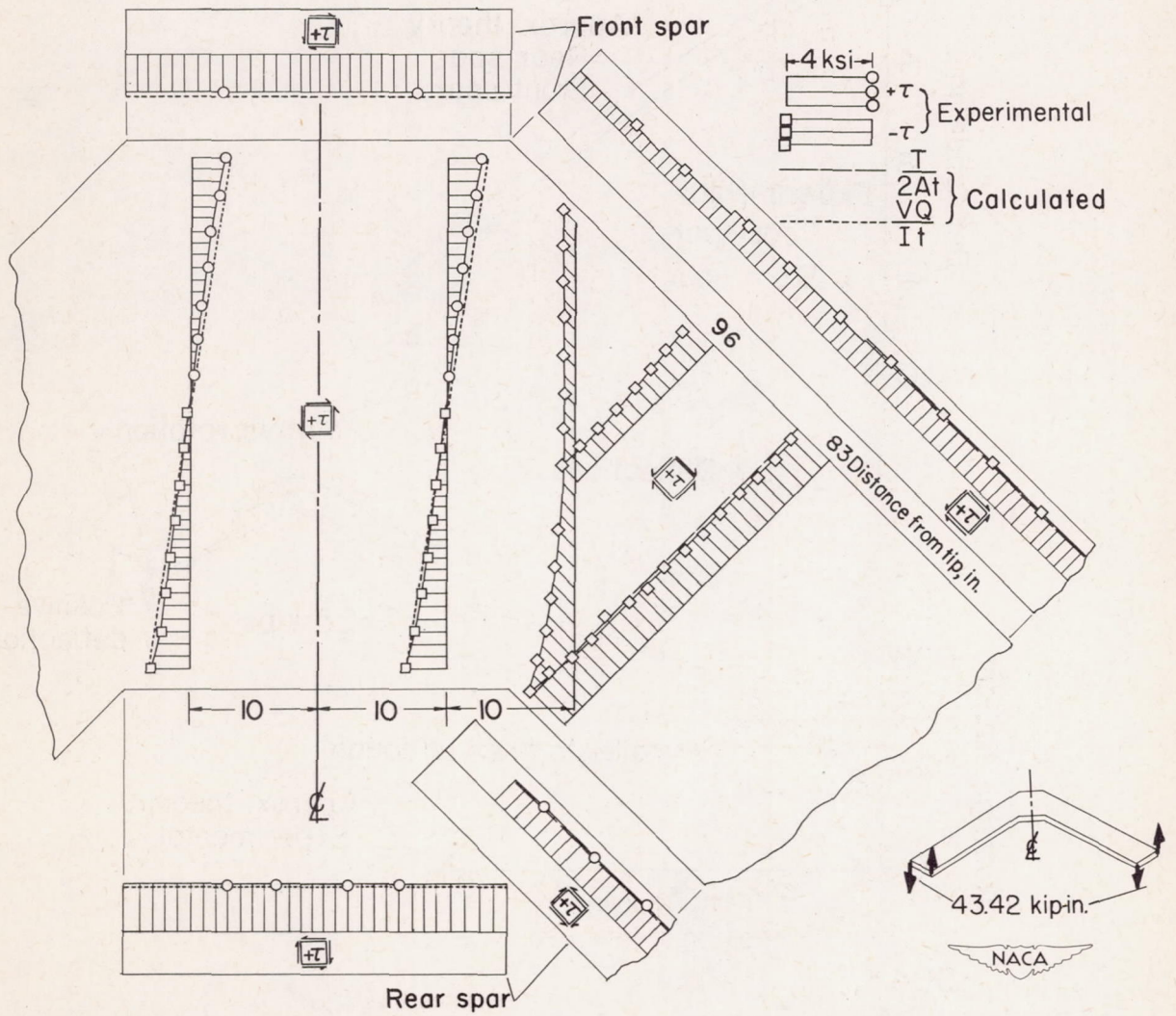


Figure 6. Shear stresses in top cover and spar webs of sweptback box beam for antisymmetrical tip torques.

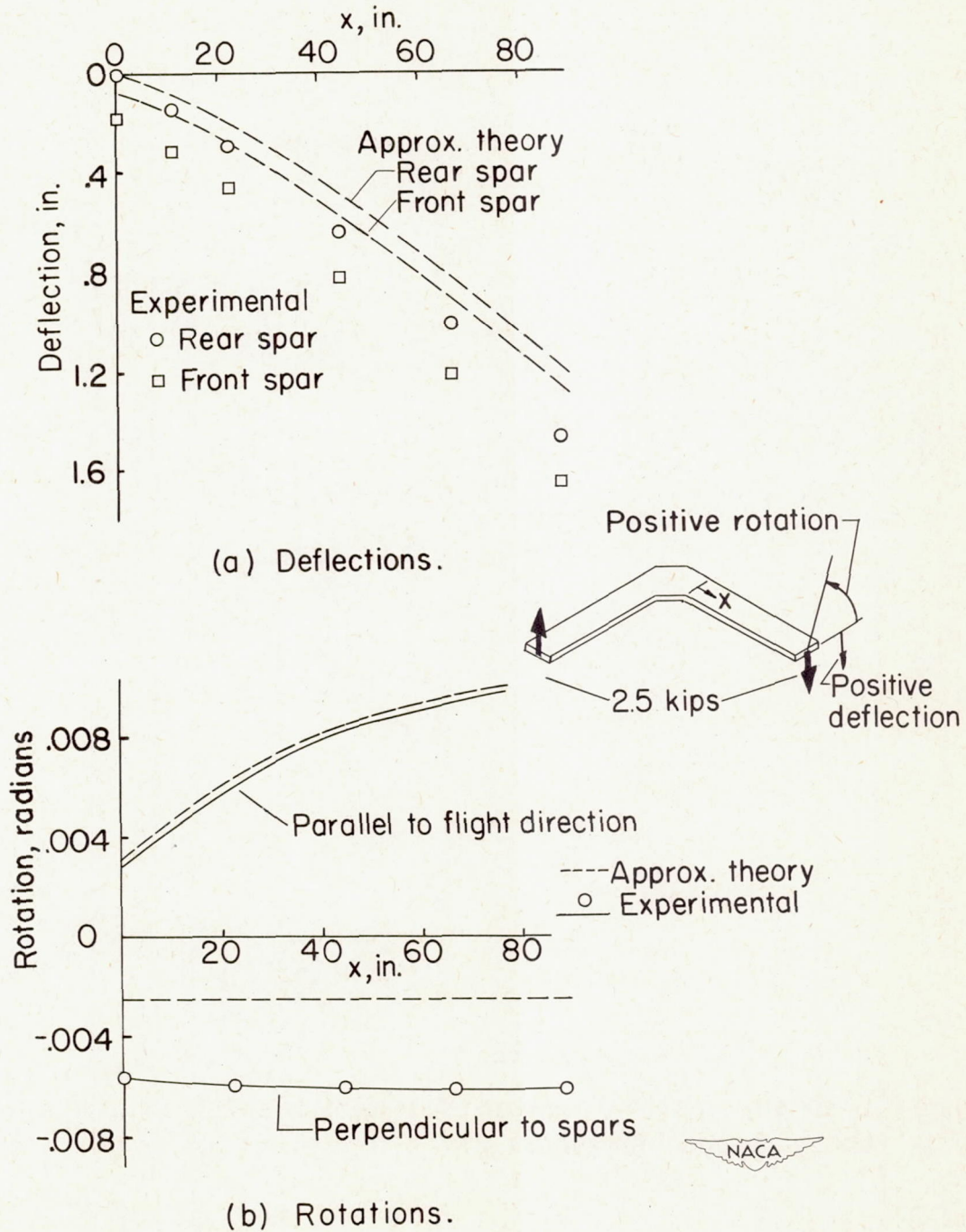


Figure 7: Distortions of sweptback box beam for antisymmetrical tip bending loads.

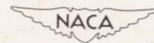
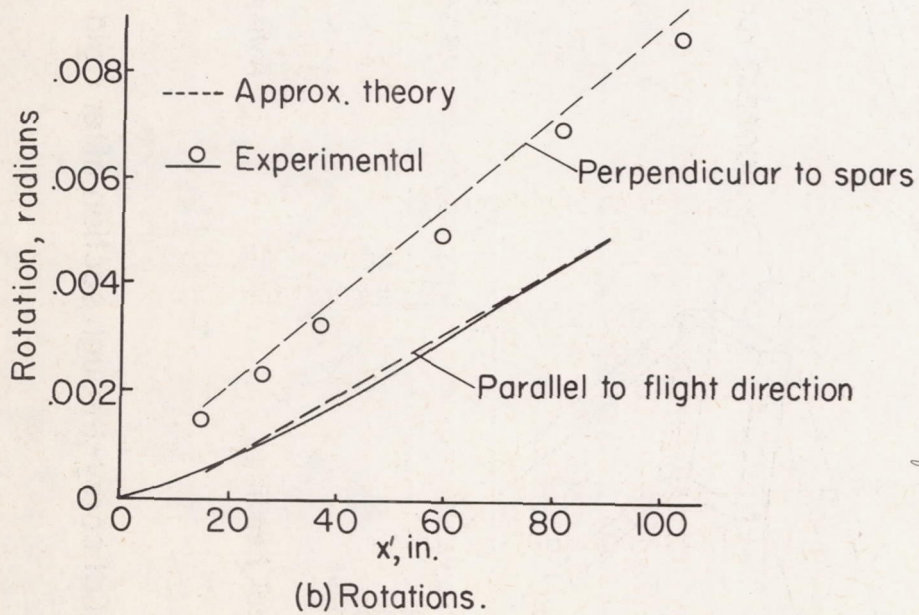
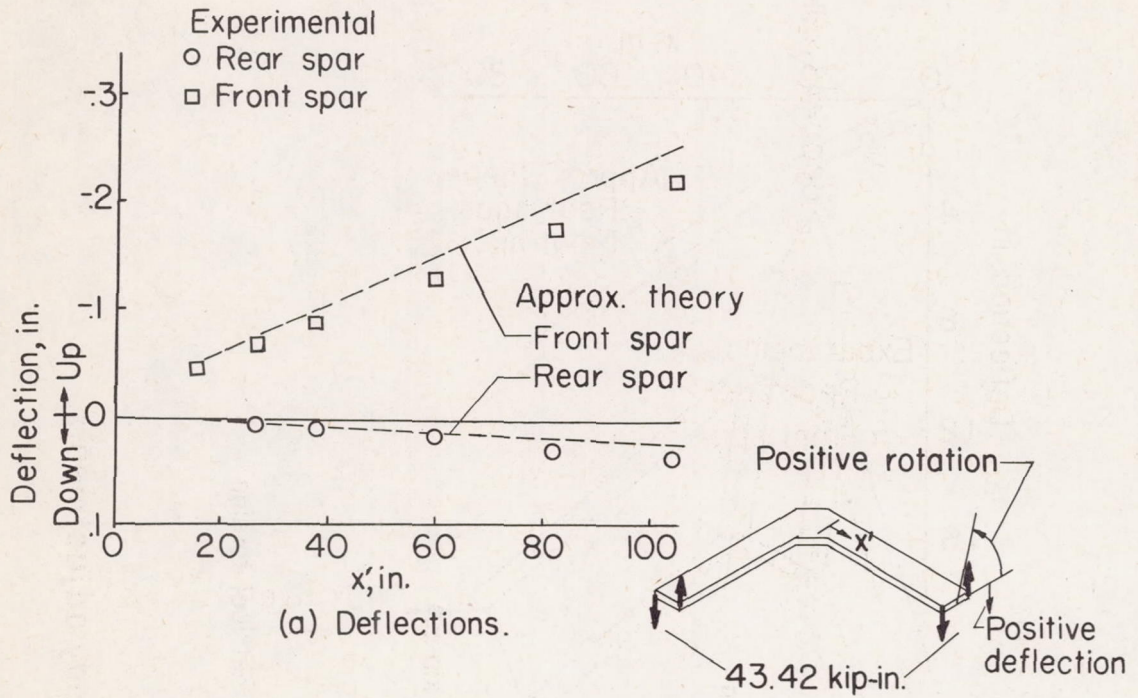
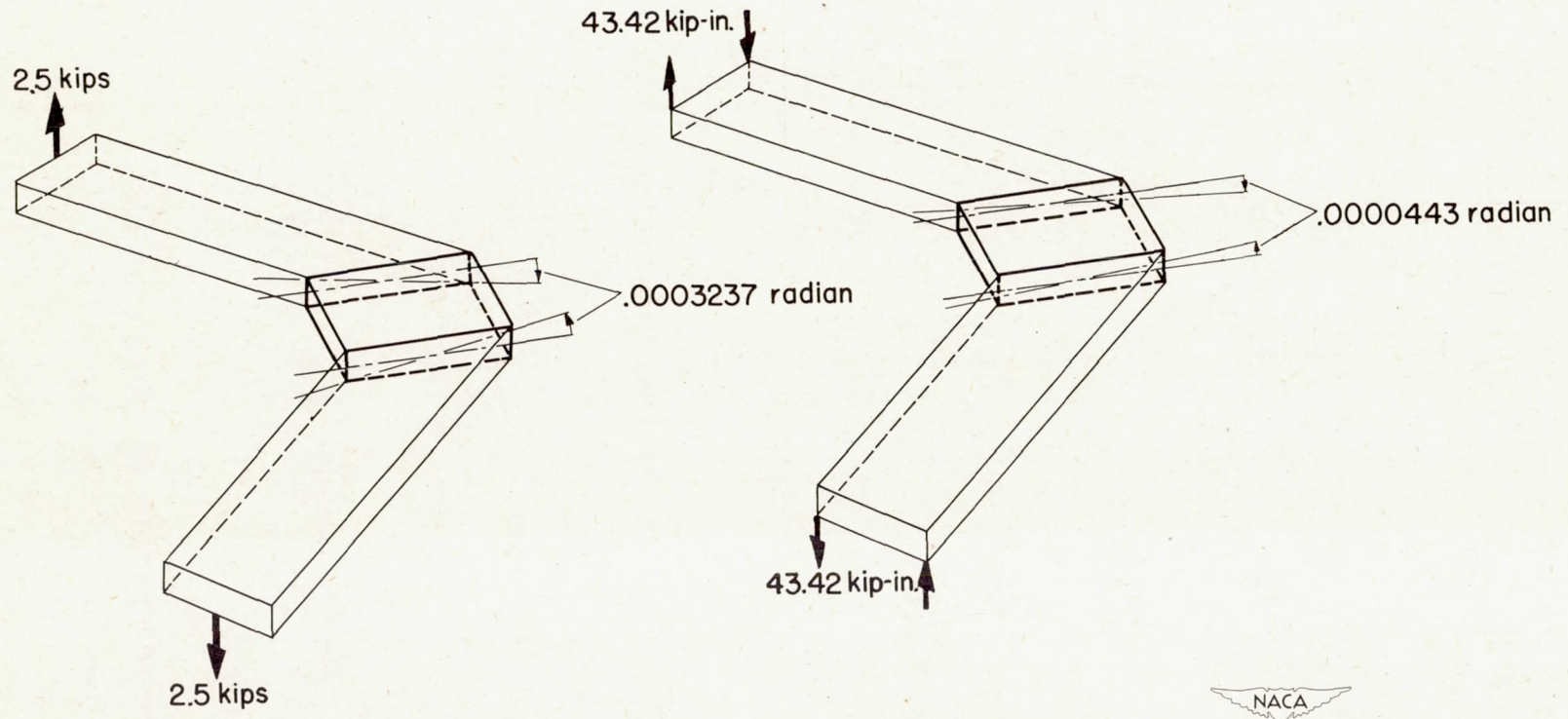


Figure 8: Distortions of sweptback box beam for antisymmetrical tip torques.



Antisymmetrical bending

Antisymmetrical torsion



Figure 9-Twist of carry-through section after rigid body adjustments.